

This is a non-peer-reviewed preprint submitted to EarthArXiv.

This manuscript has been submitted for publication in *Geophysical Research Letters*. Please note the manuscript has yet to be reviewed and formally accepted for publication. Subsequent versions of this manuscript may have slightly different content. If accepted, the final version of this manuscript will be available via the 'Peer-reviewed Publication DOI' link on the right-hand side of this webpage. Please feel free to contact any of the authors; we welcome feedback.

Unsupervised data selection for focused time-lapse inversion in electrical resistivity tomography monitoring

Thomas Hermans[1], Arne Maene[1], Corentin Caudron[2], Lore Vanhooren[1,2]

[1]Department of Geology, Ghent University, 9000 Gent, Belgium

[2]G-TIME Laboratory, Université Libre de Bruxelles (ULB), Brussels, Belgium

Abstract

Time-lapse electrical resistivity tomography has become a popular technique to monitor many subsurface processes. Inversions and interpretation often remain challenging because of the presence of noisy data and the superposition of several processes influencing the results. In this contribution, we apply for the first time clustering of data time series prior to the inversion process. We then invert only for a subset of data points displaying some interesting temporal variations. This approach allows to reduce data misfit within the data subset and successfully isolate the main processes from other taking place along the measuring profile. This opens new perspectives for the processing of time-lapse ERT data and the monitoring of subsurface processes.

Keywords

Electrical Resistivity Tomography, Clustering, time-lapse inversion, data misfit, long-term monitoring

Highlights

1. Unsupervised clustering is used to select subsets of time-lapse ERT monitoring data showing interesting temporal trend
2. Selected subsets are inverted separately to focus imaging and identify the origin of the signal
3. Results show that the approach is efficient to remove secondary variations from the image and reduce data misfit

1. Introduction

Long-term monitoring of subsurface processes using time-lapse electrical resistivity tomography (TLERT) has gained popularity in the last two decades thanks to the development of fully-automated and energetically autonomous systems. (Slater and Binley, 2021; Dimech et al., 2022; Hermans et al., 2023). Long-term data sets pose several challenges in terms of inversion: the choice of the inversion method strongly impacts the recovered resistivity (e.g., Singha et al., 2015; Dimech et al., 2022); varying noise level is difficult to handle (Lesparre et al., 2017); and finally, interpretation of inverted resistivity is not straightforward, since long-term changes in resistivity are impacted by several factors such as pore water salinity, gas, water and non-aqueous phase liquid saturations, temperature, dissolution, precipitation and alteration processes (Hermans et al., 2014; Singha et al., 2015; Slater and Binley, 2021) and that several processes are often superimposed (e.g., Hayley et al., 2010; Hermans et al., 2012; Delforge et al., 2021). In addition, different parts of the an ERT profile can be affected differently by these processes making interpretation extremely difficult (e.g. Dumont and Singha, 2024).

The need to refine ERT imaging and interpretation led several authors to propose clustering approaches on resistivity time series from TLERT. The objective is often to identify zones with similar trends and disentangle superimposed subsurface processes. Delforge et al. (2021) tested several clustering approaches to identify different hydrofacies in a karstic system based. They applied normalization and dimension reduction to improve the efficiency, leading to the identification of various trends in the resistivity images linked to infiltration processes. Gonzalez and Misra (2022) applied k-means clustering combined with dynamic time wrapping to image carbon storage. They optimize the number of clusters based on the Davies-Bouldin index. Herui et al. (2022) also applied clustering to identify water inrush into coal mines while Singley et al. (2022) applied hierarchical clustering for processes in the hyporheic zone and Chen et al. (2024) during heating experiments.

Cozzolino et al. (2020) proposed to select a subset of the original data sets to better delineate resistivity anomalies in static surveys. They show consistent resistivity distributions can be obtained from reduced data sets. Their data subset however is purely based on the location of data points within a horizontal window in the pseudosection. Since inversion approaches are based on a global convergence criterion

towards a target data misfit, some parts of the dataset might be overfitted while others are underfitted. Inverting for subsets of data would allow in principle to fit the selected data to their noise level, reducing over- or underfitting.

In this contribution, we apply clustering on TLERT resistance data time series rather than inverted resistivity sections. Data clustering is fully data-driven, allowing the selection of data points only with an interesting temporal behaviour. Doing so, the origin of this signal is better identified and disentangled from other processes taking place at other locations along the ERT profile. Inverting only the selected clusters improves the data misfit, leading to improved inversion results crucial for quantitative interpretation. We demonstrate our approach on TLERT data collected on an active hydrothermal system. To our knowledge, this is the first time clustering of resistance time series is applied prior to inversion. Our proposed methodology opens new perspectives for the processing and quantitative interpretation of long-term TLERT data sets.

2. Methodology

2.1. Subset selection

Long ERT time series often contain outliers related to bad measurements (Figure 1E). To avoid their influence during the clustering, we first carry out an outlier filtering step. We calculate the distance between percentiles 15 and 85 for each time series. All measurements falling outside 1.5 this range are identified. Since some interesting features in the data would be identified as outliers with this criterion alone, when the previous and next days are also identified as outliers, this points towards interesting features in the data sets. Only isolated outliers are removed. For the purpose of subset selection, outliers are then replaced by the linear interpolation of resistance value from the previous and next days.

The time series are normalized to avoid an excessive impact of the amplitude of the resistance on clustering results. We use two normalization approaches. The first one is the min-max normalization, in which the amplitude of each time series is rescaled to vary between 0 and 1 so that absolute variations have less influence on the selection

$$R_{norm}(t) = \frac{R(t) - \min(R(t))}{\max(R(t)) - \min(R(t))} \quad (1)$$

where $R(t)$ and $R_{norm}(t)$ are the measured and normalized resistance time series respectively, and min and max the minimum and maximum value of the time series. The second one is a normalization of the time series to a zero-mean unit-variance distribution which is not bounded:

$$R_{norm} = \frac{R(t)-\mu_R}{\sigma_R} \quad (2)$$

where μ_R and σ_R are the mean and standard deviation of the time series respectively. The next steps of the selection are applied separately on the two normalized resistance series, and then merged before inversion.

Since TLERT data sets contains a lot of redundancy, both in time and space, we reduce the dimension of the data before clustering. We opted for multi-dimensional scaling (MDS) as an effective dimension reduction technique (Lopez-Alvis et al., 2019). The Euclidean distance between every pair of normalized time series is calculated to populate a distance matrix. The distance matrix is then mapped in a lower dimensional Cartesian space by optimizing a stress function ensuring the initial Euclidean distance matrix is well approximated (De Leeuw and Heiser, 1980). MDS is preferred over principal component analysis for its ability to capture non-linearity within the data (Lopez-Alvis, 2019) which is confirmed by the explained variance retained in the 3 first dimensions (> 95%).

Finally, k-means clustering is applied in the MDS space to group data points that are close to each other. The number of clusters is selected according to the silhouette index (Kaufman and Rousseuw, 1990). The time series are analyzed to identify the cluster(s) containing interesting features. While the methodology can be classified as unsupervised learning, this last step requires input from the user to select which clusters should be selected.

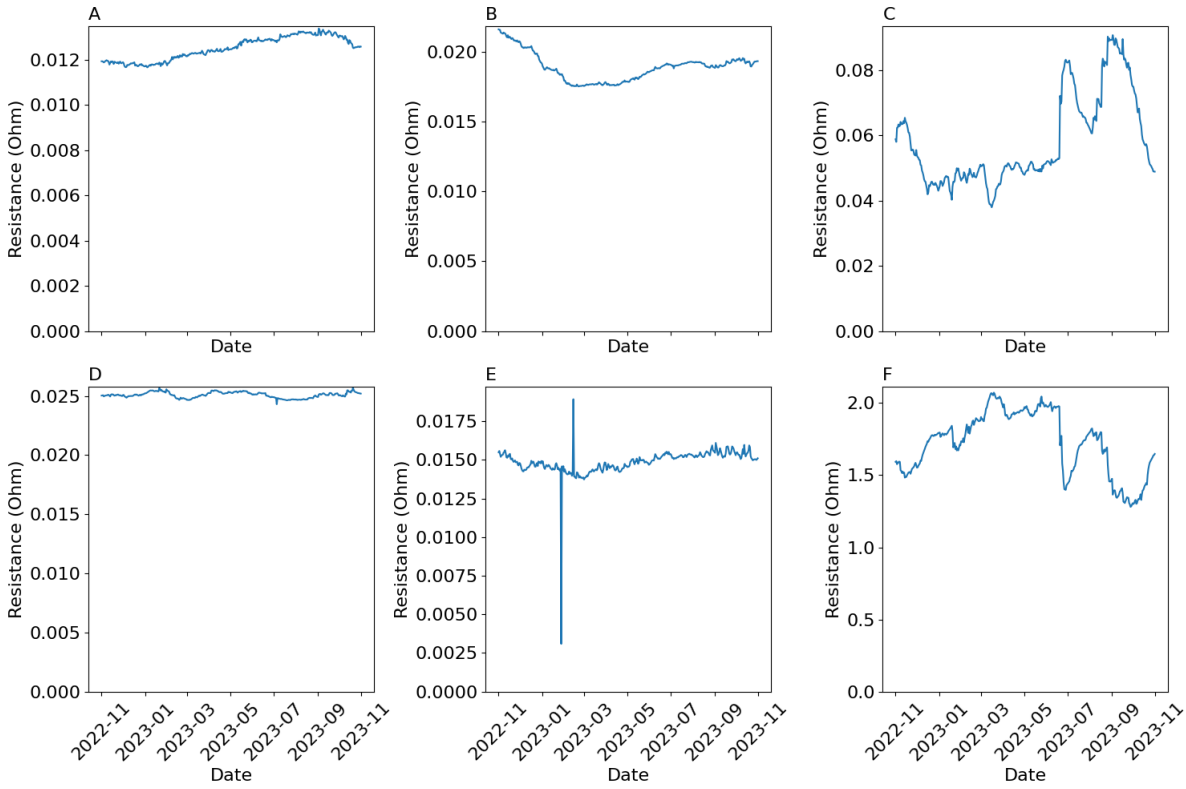


Figure 1. Example of time series contained in the data set. Some data sets show seasonal (A) or long-term (B) trends or some punctual anomalies (D). Some data sets show the clear presence of outliers at specific dates (E). Some data sets show event-related anomalies occurring at specific time (C and F) that are of interest in this study.

2.2. Inversion

In this paper, we used the time-constrained inversion (e.g. Miller et al., 2008) to invert the TLERT data sets. This approach generally allows to reduce artefacts of inversion by minimizing the difference with a reference model. The objective function of the regularized inversion problem is expressed as (Hermans and Paepen, 2020):

$$\phi(\boldsymbol{m}) = \|W_d(\boldsymbol{d} - f(\boldsymbol{m})\|_2 + \lambda(\|W_m(\boldsymbol{m} - \boldsymbol{m_0})\|_2 + \alpha\|\boldsymbol{m} - \boldsymbol{m_0}\|_2) \quad (3)$$

where $\boldsymbol{m}$ is the natural logarithm of the resistivity value in each cell of the model, $\boldsymbol{d}$ is the natural logarithm of the measured resistance, f is the forward model, W_d is the data weighting matrix, a diagonal matrix whose elements are the inverse of the estimated error e, W_m is the roughness matrix, calculating the gradients in model $\boldsymbol{m}$, and $\boldsymbol{m_0}$ is the reference model. λ is the regularization factor, balancing between the data misfit and model misfit terms, while α is the closeness factor for the reference model. The error is expressed using a linear error model

$$e = a + bR \quad (4)$$

where a is an absoluter error component, and b is a relative error component expressing that the error typically increases with the measured resistance R. The reference model is chosen as the inverted model obtained for the background data set, using the same objective function but with no reference model.

All inversions are performed using CRTomo (Kemna, 2000). CRTomo uses a Gauss-Newton iterative scheme for minimizing the objective function and a line search to optimize λ at each iteration. The inversion stops when the error weighted root-mean-square error ϵ_{RMS} reaches 1 meaning that the data set is globally fitted to its expected error level (Thibaut et al., 2021):

$$\epsilon_{RMS} = \sqrt{\frac{1}{N}\sum_{i=1}^{N}\frac{\left(d_i - f_i(\boldsymbol{m})\right)^2}{e_i^2}} \qquad (5)$$

where N is the number of data points. A robust data constraint is used to limit the impact of outliers on the solution (Kemna, 2000).

To compare the results between several inversion within the selected clusters, the individual residual and relative errors are also computed:

$$\epsilon_{ind,i} = d_i - f_i(\boldsymbol{m}) \qquad (6)$$

$$\epsilon_{rel,i} = \frac{d_i - f_i(\boldsymbol{m})}{d_i} \times 100 \qquad (7)$$

3. Results

3.1. Field site and data set

We illustrate the proposed methodology using a data set collected in Iceland within the context of the monitoring of a hydrothermal system, located on the Reykjanes peninsula (Iceland) in the vicinity of the Gunnhuver hot spring (Figure S1). A 72-electrodes 355 m-long ERT profile was installed in a zone containing several hydrothermal features and inactive portions (Vanhooren et al., 2025). The data are collected using a multigradient protocol from November 2022 from 1 year. Until June 2023, only small scale variations are observed (Figure 1). In June 2023, some of the measured quadrupoles start to display strong positive or negative anomalies whose amplitude is often larger than other events in the time series, culminating in two peaks during the summer. Since this period corresponded with a strong volcanic activity in the Reykjanes peninsula, we want to isolate the quadrupoles affected by these peaks and better understand the processes at their origin.

3.2. Subset selection

K-means clustering is applied on the MDS maps obtained from the distance matrices obtained with the two types of normalization (Figure 2). In both cases, the optimum number of clusters is 6. The pseudosection of clusters indicate both normalizations globally recover similar patterns in the data. Clusters 0 and 1 from the min-max normalization are relatively equivalent to clusters 4 and 0 from the 0-mean unit variance method. They contain data points displaying a clear trend in which positive or negative peaks of resistance are observed. They are mostly located in the right part of the pseudosection. The data points with negative peaks are mostly very shallow, while the points with positive peaks are found deeper. They correspond to the behaviour we identified previously in Figures 1.

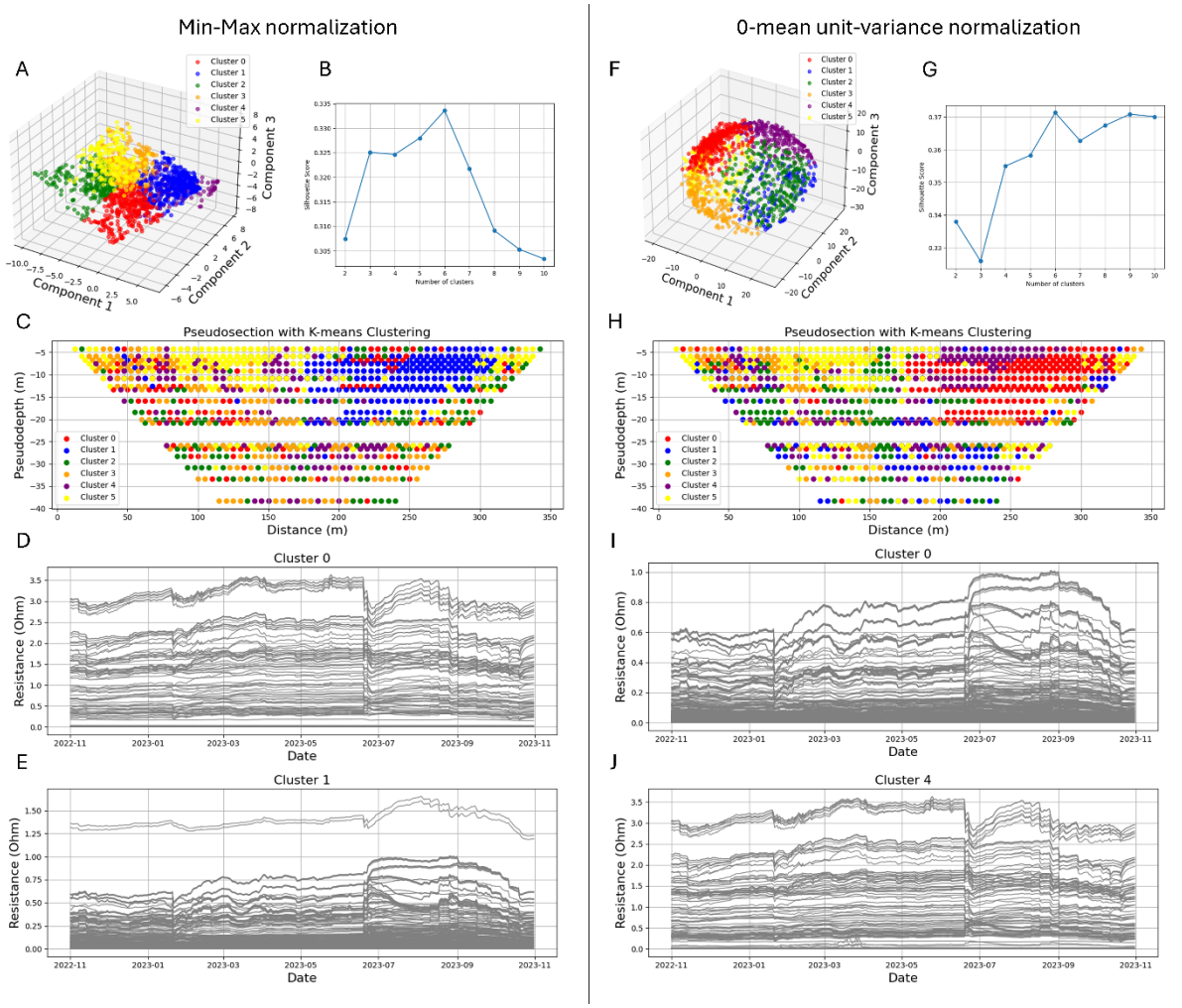


Figure 2. Clustering results for the min-max normalization (left) and the 0-mean unit-variance normalization (right). Clusters in the 3 dimension MDS space (A and F), Silhouette index indicating the optimum number of clusters (B and G), pseudosection with spatial distribution of the clusters (C and H) and resistance series in the selected clusters (D, E, I and J).

Nevertheless, we also observe isolated points in the pseudosections, and points which do not really have the same temporal trends as others after clustering (Figure S2). This is a consequence of k-means clustering in which points are classified based on their distance to the cluster center, inducing uncertainty at the cluster boundaries. We therefore combine the results of both normalization procedures, and keep only the datapoints that belong to the selected clusters for both approaches. Some points having the desired trend are omitted, but the impact remains limited as ERT data sets are known to contain a lot of redundancy. The selected subset contains 625 quadrupoles out of the 1624 initial ones, i.e. 38.5% of all data points.

3.3. Inversion

We invert a profile every 10 days until the end of October, resulting in 16 data sets. The full data set of June 1 is used as a reference for the time-constrained inversion. The closeness factor α is fixed to 0.3. The results for each time step ρ_i are displayed as percentage change in resistivity $\Delta\rho$ in comparison to the inversion results of June 1 obtained through the time-constrained inversion (ρ_0):

$$\Delta\rho = \frac{\rho_i - \rho_0}{\rho_0} \times 100 \qquad (8)$$

The inversion results for the full and selected data sets are compared for 5 selected dates (Figure 3). With both data sets, the image is dominated by strong changes in resistivity up to more than 150% between 150 and 300 m along the profile. The changes are negative (lower resistivity) in the shallow part and positive in the deeper part. These anomalies are the results of the peak of resistance observed in the data set. They appear around June 20, reach a first peak around July 10, evolve towards a local minimum on July 30, rise again until August 30 and then slowly decrease to the initial level at the end of October. This zone has a higher elevation on the profile, and is characterized by an absence of hydrothermal alteration features at the surface (Vanhooren et al., 2025).

A notable difference in the results is that the inversion with the full data set also contain changes in resistivity in the first 150m of the section, which is hydrothermally active. Their amplitude is lower (limited between -30 and +50 %) and are more localized. Changes of resistivity in the very shallow layers are also present. These changes are typical of the hydrothermal activity of the site, and can be observed all year long. Since they are not part of the selected clusters, these variations are absent of the

inversion with the selected data set in which only the anomalies related to the peaks can be observed. A single other location, around 50 m, also shows some variations of resistivity. It corresponds to some data points which also display the peak behaviour and were selected with both normalization approaches. The cumulative sensitivity (Figures 3F and 3L) indicates that the selected data set still has sensitivity close to the surface in this zone. The amplitude of the changes is however much smaller.

Another difference in the results is the amplitude and spatial extent of the changes in resistivity obtained with the two data sets. Both tend to be larger for the selected data sets, especially during the period of maximum changes.

The selection of a subset of the data based on clustering successfully identifies the desired process and lead to a more focus imaging of the related processes. It allows us to conclude that the presence of the peak is limited to a specific area of the profile which is not visibly active. This cannot be easily concluded from the full data set as the inverted results show changes in resistivity everywhere, including in hydrothermally active zones. The presence of several processes acting simultaneously would render the quantitative interpretation difficult, but the proposed approach enables us to derive more focus images.

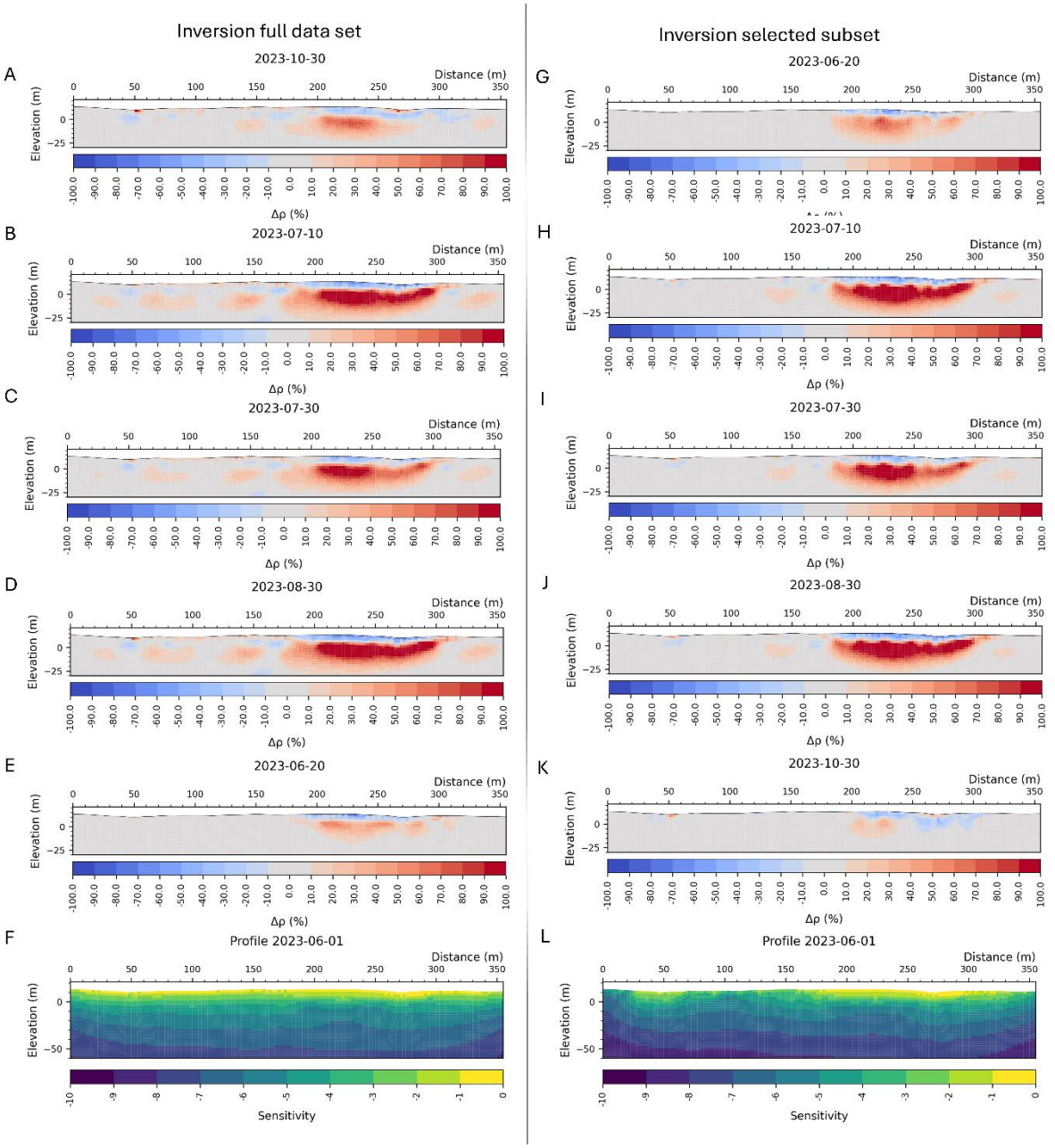


Figure 3. Inversion results with the full data set (left) and the selected subset (right) on June 20 (A and G), July 10 (B and H), July 30 (C and I), August 30 (D and J), October 30 (E and K) and normalized cumulative sensitivity (F and L).

3.4. Data misfit

The difference in recovered change of resistivity between the two data sets is intimately linked to the inversion approach. The convergence criterion is related to the solution reaching an error corresponding to its noise level (e.g., Thibaut et al., 2021), ensuring that the data set is not globally over- or underfitted. However, this global fit is an average over the whole data set, some points with a better or lower fit compensate each other.

This is actually observed for the full data set. The ϵ_{RMS} for the selected quadrupoles using the normal scale and the natural logarithm scale (Table 1) is systematically better for the selected data set in the resistance scale, and for most dates in the in the log scale. The differences are not significant in the early time-steps, before the resistance changes. In the period of maximum variations (July-August), the inversion of the full data set leads to underfitting of the data within the cluster, with ϵ_{RMS} for the logarithmic scale values largely above 1, while the values for the selected data set are very close to 1. Although CRTomo applies $\epsilon_{RMS} = 1$ strictly, the deviations in Table 1 originate from the robust data constraint, adapting noise estimate to accommodate outliers (Kemna, 2000). The full data set globally leads to a worse fit of the peaks, which is compensated in the inversion by an overfitting of quadrupoles in other areas along the profile.

Table 1. Data misfit.

DATE	FULL INVERSION	FULL INVERSION LOG SCALE	SUBSET INVERSION	SUBSET INVERSION LOGSCALE
01/06/2023	2.715	0.904	2.156	0.891
10/06/2023	2.663	1.108	3.339	1.468
20/06/2023	2.147	0.683	1.877	0.832
30/06/2023	2.899	0.785	2.647	1.131
10/07/2023	**2.982**	**0.875**	**2.63**	**0.847**
20/07/2023	**3.265**	**1.443**	**2.767**	**1.108**
30/07/2023	**3.255**	**1.477**	**2.766**	**0.915**
10/08/2023	**3.171**	**1.577**	**2.825**	**1.104**
20/08/2023	**3.022**	**1.274**	**2.776**	**1.473**
30/08/2023	**3.185**	**1.267**	**2.679**	**0.851**
10/09/2023	3.220	1.073	2.715	0.866

20/09/2023	3.155	0.988	2.750	0.774
30/09/2023	3.343	1.257	2.757	0.864
10/10/2023	2.269	0.936	2.649	0.937
20/10/2023	3.833	1.760	2.669	1.242
30/10/2023	3.692	1.701	2.295	1.354

This is confirmed by the analysis of the individual and relative error (Figure 4). The improved fitting is clearly present when inverting the selected data set alone. The relative error decreases in deep parts of the pseudosection, where the measured resistance is low, and for the shallowest data points characterized by negative peaks. In contrast, the absolute error decreases more significantly in the upper part of the pseudosection where resistance are higher. The recovered resistivity changes in the identified zone are more reliable estimations of the actual true variations in the subsurface, explaining why the absolute values of the change in resistivity have a larger amplitude when inverted with the selected subset (Figure 3).

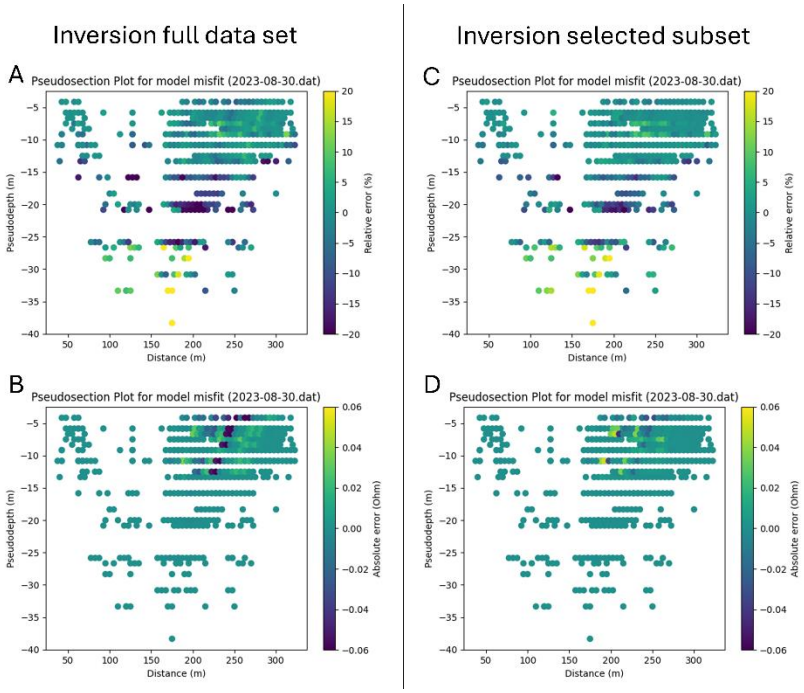


Figure 4. Data misfit for the inversion of August 30 with the full (left) in selected data sets (right) expressed in relative error (A and C) and absolute error (B and D).

The increase in resistivity at depth is likely related to a higher gas saturation. This could be related to gas trapping below a capping layer, a phenomenon used to explain hydrothermal eruptions (Christenson

et al., 2010). The decrease of resistivity in the surficial zone would be rather related to temperature increase, as the higher gas flux in the hydrothermal system would be accompanied by a higher heat flux. In active zones, more permeable discharge pathways for gas exist, so that changes in resistivity do not reach a level as high as in the non-active zone. This hypothesis should be validated by additional data and modelling, but this falls out of the scope of this paper.

4. Conclusion

Monitoring subsurface processes with TLERT has become popular in the past decades. However, disentangling the origin of resistivity changes remains a difficult task owing to the variety of factors affecting bulk resistivity. In this paper, we select a subset of the full data set based on the temporal behaviour of measured resistance. The resistance time series for each quadrupole are first normalized and projected in a lower dimensional space using MDS. Data points are clustered in the lower dimensional space and only clusters showing interesting temporal behaviour are selected for inversion. The methodology is fully unsupervised and automated, including the selection of the number of clusters. Only the identification of the clusters used for inversion requires expert input.

The inversion results for the selected subset compared to the full data set show that 1) the qualitative evolution of resistivity in the zone of interest is not affected, indicating that no information is lost in the selection process; 2) resistivity variations having other trends are successfully removed from the final images, allowing to focus the interpretation on the process of interest; 3) the data misfit in the selected clusters is smaller when inverted alone, leading to a global improvement in the recovered resistivity changes, and making *in fine* a more quantitative interpretation possible.

The proposed methodology has the potential to be broadly applied in TLERT when several processes affecting the resistivity are occurring along the monitored profile. The inversion of selected clusters should not replace inversion of the full data sets, but should be applied after identification of interesting signals to refine imaging. It could for example be applied in coupled inversion scheme to reduce the computational cost of the forward problem. Future work could focus on more advanced clustering approaches, including unsupervised and supervised machine learning, to avoid the presence of outliers within the selected clusters, or of missing interesting points wrongly classified in unselected clusters.

Author CRediT

TH: Conceptualization, Formal Analysis, Funding Acquisition, Methodology, Project Administration, Visualization, Supervision, Writing – Original Draft; **AM**: Data Curation, Formal Analysis, Visualization; **CC**: Conceptualization, Funding Acquisition, Supervision, Writing – Original Draft; **LV**: Data Curation, Formal Analysis, Methodology, Visualization, Writing – Original Draft;

Acknowledgment

This study is carried out within the project ERUPT funded by the Flemish Fund for Scientific Research (FWO) under grant number G037222N.

Data availability statement

The datasets used for this paper are available in Vanhooren (2025). Shallow ERT and IP monitoring of the Reykjanes Geothermal Area. Zenodo, https://doi.org/10.5281/zenodo.15488867.

References

Kaufman L, Rousseuw P.J. (1990). Review of finding groups in data: an introduction to cluster analysis. https:// doi. org/ 10.2307/ 25321 78.

Slater L., Binley A. (2021) Advancing hydrological process understanding from long-term resistivity monitoring systems. WIREs Water 8(3), e1513.

Chen, H., Wang, J., Luo, L., Otto, S., Davis, J., Kuhlman, K. L., & Wu, Y. (2024). Electrical Resistivity Changes During Heating Experiments Unravel Heterogeneous Thermal-Hydrological-Mechanical Processes in Salt Formations. *Geophysical Research Letters*, *51*(14), e2024GL109836. https://doi.org/10.1029/2024GL109836

Christenson, B. W., Reyes, A. G., Young, R., Moebis, A., Sherburn, S., Cole-Baker, J., Britten., K. (2010). Cyclic processes and factors leading to phreatic eruption events: insights from the 25 September 2007 eruption through Ruapehu Crater Lake, New Zealand. *Journal of Volcanology and Geothermal Research*, 191, 15-32.

Cozzolino, M., Mauriello, P., & Patella, D. (2020). An Extension of the Data-Adaptive Probability-Based Electrical Resistivity Tomography Inversion Method (E-PERTI). *Geosciences*, *10*(10), 380. https://doi.org/10.3390/geosciences10100380

De Leeuw, J. , Heiser, W.J. (1980). Multidimensional scaling with restrictions on the configuration. In: Multivariate Analysis. North Holland Publishing Company, Amsterdam, the Netherlands, pp. 501–522.

Delforge, D., Watlet, A., Kaufmann, O., Van Camp, M., & Vanclooster, M. (2021). Time-series clustering approaches for subsurface zonation and hydrofacies detection using a real time-lapse electrical resistivity dataset. *Journal of Applied Geophysics*, *184*, 104203. https://doi.org/10.1016/j.jappgeo.2020.104203

Dumont M., Singha, K. (2024). Geophysics as a hypothesis-testing tool for critical zone hydrogeology. *WIREs Water*, 11(5), e1732.

Dimech, A., Cheng, L., Chouteau, M., Chambers, J., Uhlemann, S., Wilkinson, P., et al. (2022). A Review on Applications of Time-Lapse Electrical Resistivity Tomography Over the Last 30 Years : Perspectives for Mining Waste Monitoring. *Surveys in Geophysics*, *43*(6), 1699–1759. https://doi.org/10.1007/s10712-022-09731-2

Gonzalez, K., & Misra, S. (2022). Time-Lapse Monitoring of the Dynamic Geological Carbon Storage Using Unsupervised Spatiotemporal Clustering. *SSRN Electronic Journal*. https://doi.org/10.2139/ssrn.4156583

Hayley, K., Bentley, L. R., & Pidlisecky, A. (2010). Compensating for temperature variations in time-lapse electrical resistivity difference imaging. *GEOPHYSICS*, *75*(4), WA51–WA59. https://doi.org/10.1190/1.3478208

Hermans, T., & Paepen, M. (2020). Combined Inversion of Land and Marine Electrical Resistivity Tomography for Submarine Groundwater Discharge and Saltwater Intrusion Characterization. *Geophysical Research Letters*, *47*(3). https://doi.org/10.1029/2019GL085877

Hermans, Thomas, Vandenbohede, A., Lebbe, L., & Nguyen, F. (2012). A shallow geothermal experiment in a sandy aquifer monitored using electric resistivity tomography. *Geophysics*, *77*(1), B11–B21. https://doi.org/10.1190/geo2011-0199.1

Hermans, Thomas, Nguyen, F., Robert, T., & Revil, A. (2014). Geophysical Methods for Monitoring Temperature Changes in Shallow Low Enthalpy Geothermal Systems. *Energies*, *7*(8), 5083–5118. https://doi.org/10.3390/en7085083

Hermans, Thomas, Goderniaux, P., Jougnot, D., Fleckenstein, J. H., Brunner, P., Nguyen, F., et al. (2023). Advancing measurements and representations of subsurface heterogeneity and dynamic processes: towards 4D hydrogeology. *Hydrology and Earth System Sciences*, *27*(1), 255–287. https://doi.org/10.5194/hess-27-255-2023

Herui, Z., Guolin, W., Xiaozhen, T., & Xiaohui, Z. (2022). Distributed Fuzzy Clustering Analysis of Time-Lapse Electrical Resistivity Tomography for Water Inrush Monitoring in Coal Mines. *Sustainability*, *14*(24), 17011. https://doi.org/10.3390/su142417011

Kemna, A. (2000). *Tomographic Inversion of Complex Resistivity-Theory and Application*. Ruhr-Universität, Bochum, Germany.

Lesparre, N., Nguyen, F., Kemna, A., Robert, T., Hermans, T., Daoudi, M., & Flores-Orozco, A. (2017). A new approach for time-lapse data weighting in electrical resistivity tomography. *Geophysics*, *82*(6), E325–E333. https://doi.org/10.1190/geo2017-0024.1

Lopez-Alvis, J., Hermans, T., & Nguyen, F. (2019). A cross-validation framework to extract data features for reducing structural uncertainty in subsurface heterogeneity. *Advances in Water Resources*, *133*, 103427.

Miller, C. R., Routh, P. S., Brosten, T. R., & McNamara, J. P. (2008). Application of time-lapse ERT imaging to watershed characterization. *Geophysics*, *73*(3), G7.

Singha, K., Day-Lewis, F. D., Johnson, T., & Slater, L. (2015). Advances in interpretation of subsurface processes with time-lapse electrical imaging. *Hydrological Processes*, *29*(6), 1549–1576.

Singley, J. G., Singha, K., Gooseff, M. N., González-Pinzón, R., Covino, T. P., Ward, A. S., et al. (2022). Identification of hyporheic extent and functional zonation during seasonal streamflow recession by unsupervised clustering of time-lapse electrical resistivity models. *Hydrological Processes*, *36*(10), e14713. https://doi.org/10.1002/hyp.14713

Thibaut, R., Kremer, T., Royen, A., Kim Ngun, B., Nguyen, F., & Hermans, T. (2021). A new workflow to incorporate prior information in minimum gradient support (MGS) inversion of electrical resistivity and induced polarization data. *Journal of Applied Geophysics*, *187*, 104286. https://doi.org/10.1016/j.jappgeo.2021.104286

Vanhooren (2025). Shallow ERT and IP monitoring of the Reykjanes Geothermal Area. Zenodo, https://doi.org/10.5281/zenodo.15488867.

Vanhooren, L., Vrancken E., Dekoninck, W., Flores-Orozco, A., Fontaine, O., Bergsson, B., Jónsdóttir, K., Caudron, C., & Hermans, T. Subsurface hydrothermal alteration mapping in the Reykjanes Geothermal area using a combined geoelectrical approach. *EarthArxiv.* *https://doi.org/10.31223/X51F1K*

Supplementary information

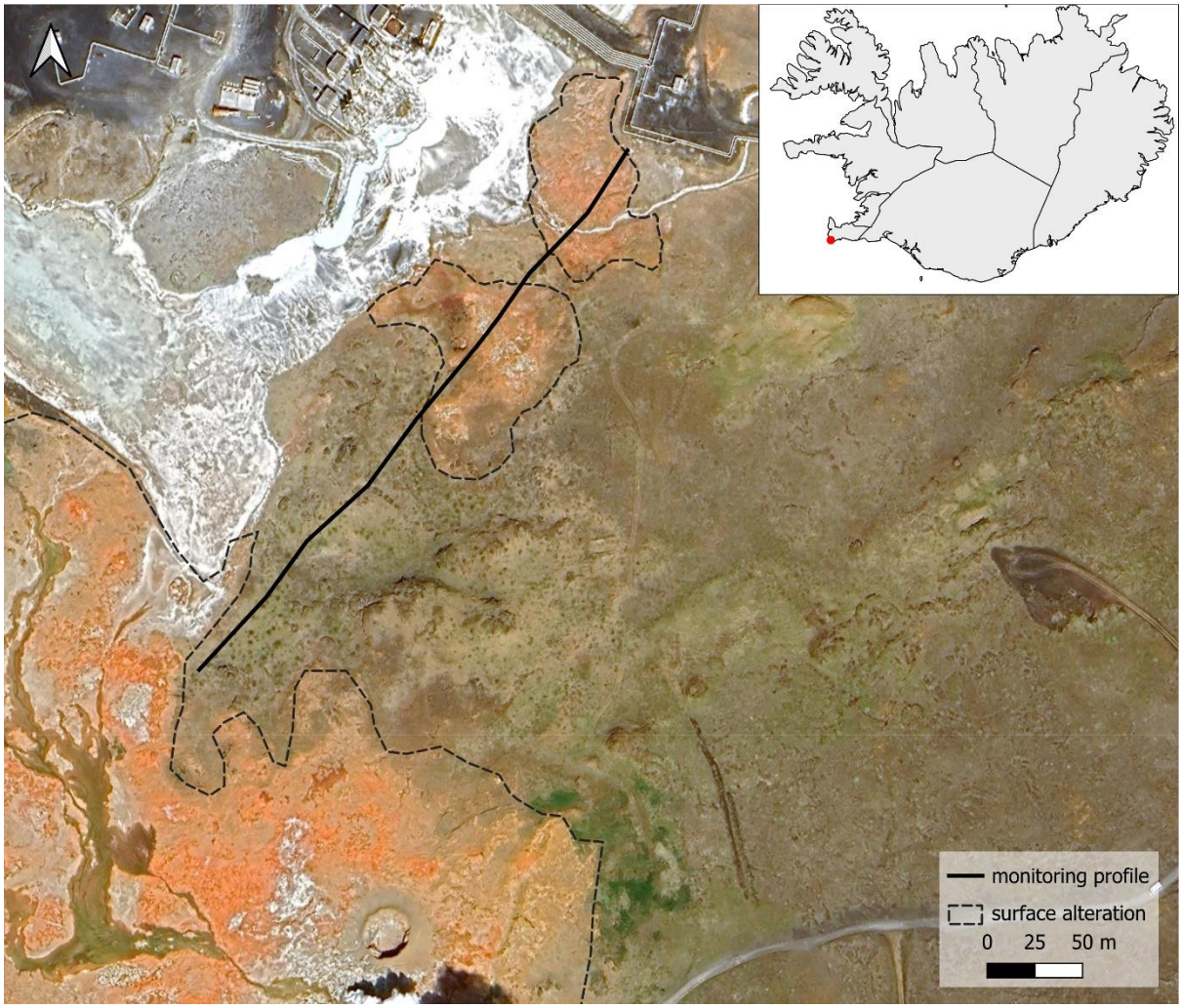


Figure S1. Localization of the study site. Electrode 1 (0 m) is located in the northern part of the site.

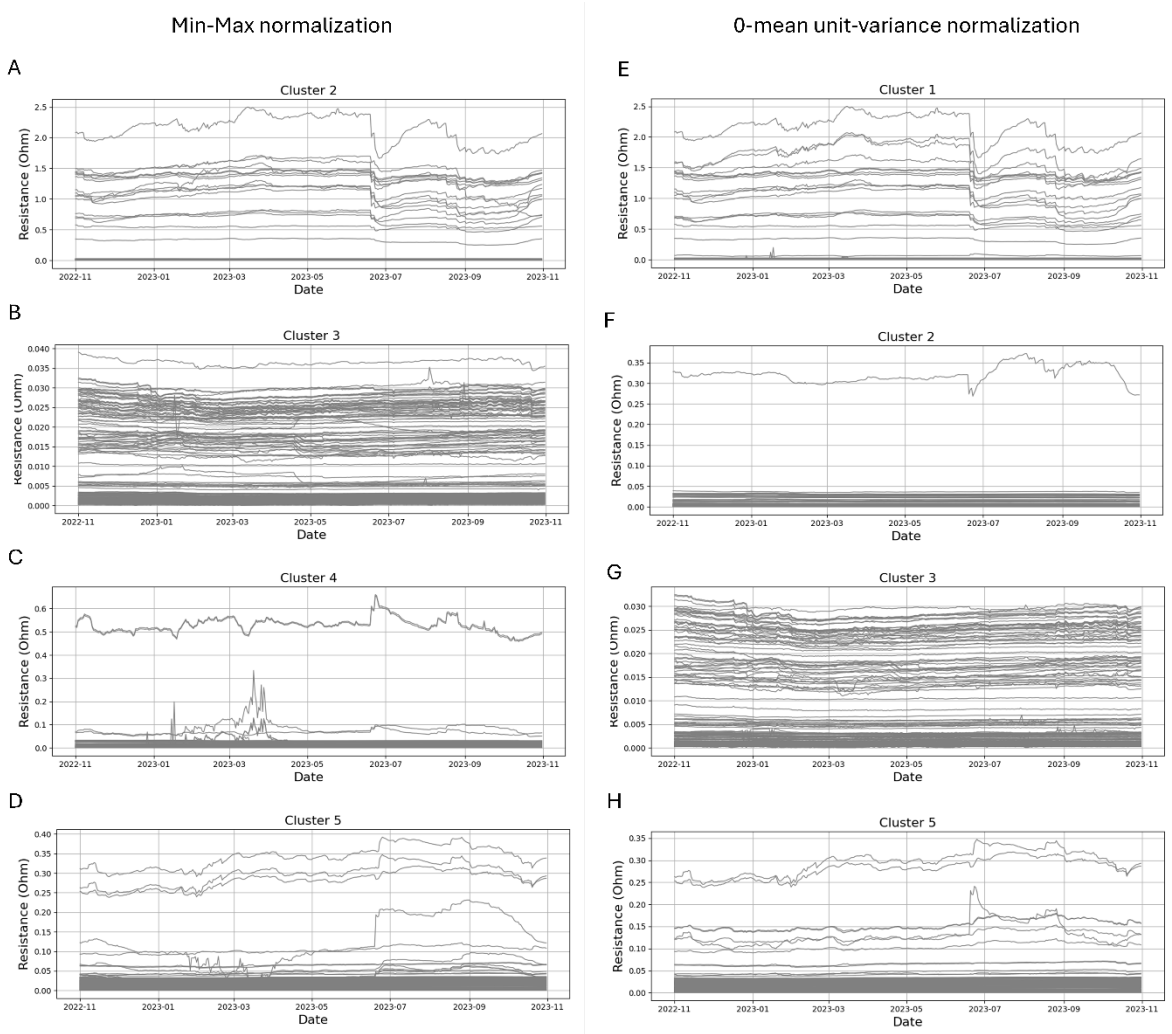


Figure S2. Resistance time series in the unselected clusters.